Local Co structure and ferromagnetism in ion-implanted Co-doped $LiNbO_3$

C. Song,[1] F. Zeng,[1] Y. X. Shen,[1] K. W. Geng,[1] Y. N. Xie,[2] Z. Y. Wu,[2] and F. Pan[1,*]

[1]*Laboratory of Advanced Materials, Department of Materials Science and Engineering, Tsinghua University, Beijing 100084, People's Republic of China*

[2]*Beijing Synchrotron Radiation Facility, Chinese Academy of Science, Beijing 100039, People's Republic of China*

(Received 5 April 2006; revised manuscript received 23 April 2006; published 22 May 2006)

A ferromagnetic oxide $Co_{0.05}(LiNb)_{0.95}O_{3-\delta}$ was prepared by Co ion implantation into (104) $LiNbO_3$ wafers. Co is uniformly distributed to a depth of ~220 nm by implanting at three different energies and doses. Electron energy loss spectroscopy and x-ray absorption near-edge structure (XANES) spectra reveal a solid solution of cobalt in an implanted layer, where Co is not metallic but in the 2+ state. Furthermore, full multiple-scattering *ab initio* calculations of Co XANES at the *K* edge clearly provide a structure fingerprint to determine Co substitution at Li lattice sites rather than Nb. The $Co_{0.05}(LiNb)_{0.95}O_{3-\delta}$ system exhibits room temperature ferromagnetism of $1.3\mu_B$/Co ion with an easy in-plane axis and a high Curie temperature of 710 K.

DOI: 10.1103/PhysRevB.73.172412 PACS number(s): 75.30.−m, 78.70.Dm

Diluted magnetic semiconductors (DMSs) have received much attention within the emerging field of spintronics.[1] By employing some synthesis techniques, such as pulsed-laser deposition,[2,3] molecular beam epitaxy,[4] and magnetron sputtering,[5] a number of diluted magnetic systems have been obtained.[2–8] Ion implantation, which is known to introduce species above the usual equilibrium solubility limit, provides an alternative way to investigate DMSs.[9–14] Also, this technique is compatible with standard semiconductor processing. However, the distribution and phase of the implanted ions are critically influenced by the implantation parameter. Most of the previous studies were performed by a single energy and a certain ion dose, which lead to the Gaussian distribution of implanted ions.[9–13] The resulting magnetic properties (i.e., ferromagnetism[9–12] and paramagnetism[12,13]) arising from the high doping ions concentration or the low concentration are ambiguous. It is hence of importance to achieve uniform doping ions distribution by a series of designed energies and the corresponding doses of ion implantation.[14]

$LiNbO_3$ (LNO) has been selected as a host of magnetic oxides in this work for two reasons. First, LNO is a ferroelectric crystal which is of particular interest for photorefractive devices, optical waveguide, and surface acoustic wave filters.[15–19] Taking into account of ferromagnetism introduced by Co ion implantation, it could exhibit promising multiferroic properties, similar to $BiFeO_3$.[20] Second, previous works revealed that impurities had an important effect on the electro-optic properties of LNO.[16–19] To fully understand the optical modifications introduced by the impurities, their lattice locations were characterized by several methods, such as electron spin resonance,[16,17] extended x-ray-absorption fine-structure,[18,19] and Rutherford-back scattering.[21] These measurements indicate that the lattice location of transition-metal (e.g., Mn, Fe, Ni) and rare-earth ions (e.g., Eu) show trigonal C_3 symmetry and favor a particular site, i.e., Fe is most likely to site in a Li position.[18] Nevertheless the determination of the local geometry of impurities is generally hindered by both Li and Nb sites that lie on a threefold axis and by other special reasons such as the radii of Li^+ and Nb^{5+} are very close to each other.[16,17] Clearly, there is a pressing need for an in-depth reality check of the previous concepts and a more accurate method to elucidate the hyperfine structure. The X-ray absorption near-edge structure (XANES) is currently of great interest due to its promise of providing local chemical information in complex materials and it is sensitive to subtle differences of local arrangement.[22] More importantly, the XANES spectrum and its interpretation are intimately related to ground-state electronic structure,[22–24] which is of help for better elucidation of the impurities substitution at Li ($1s^2 2s^1$) or Nb ($4d^4 5s^1$).

(104) LNO wafers were implanted with a combination of Co ions to 1.3×10^{16} cm^{-2} at 300 keV, 0.54×10^{16} cm^{-2} at 110 keV, and 0.19×10^{16} cm^{-2} at 30 keV, which is calculated by TRIM (transport and range of ions through matter) beforehand. During implantation, no special heating or cooling was provided to the sample holder (Cu foil). High resolution transmission electron microscopy (HRTEM) imaging, selected area electron diffraction (SAD), energy dispersive spectrometer (EDS), and electron energy loss spectroscopy (EELS) were used to study the structural characteristics. Co *K*-edge XANES spectra were measured in the fluorescence mode using synchrotron radiation with Si(111) double crystal monochromator at the beam line 4W1B of the Beijing Synchrotron Radiation Facility (BSRF). The storage ring worked at a typical energy of 2.2 GeV with an electron current of ~100 mA. The spectra were scanned in the range of 7.5–8.0 keV with steps of 0.5 eV and an energy resolution of 1.5 eV. Common background subtraction was employed in the data reduction and the data were normalized and calibrated to the edge of the Co metal foil. Magnetization studies were carried out using a superconducting quantum interference device (SQUID) magnetometer in the temperature range of 5–350 K. High temperature magnetization ($300 < T < 750$ K) was recorded using a vibrating sample magnetometer (VSM).

Co *K*-edge XANES spectra have been simulated via the full multiple-scattering (MS) theory using the *ab initio* self-consistent free energy force field (FEFF) 8.2 code with two complementary modes: MS scattering and path analysis by examination of only the most important scattering paths.[22] Within the FEFF code, exchange parameters were adjusted to correct for any offset in the calculated Fermi energy level, generally a negative shift of 3 eV. For the exchange-

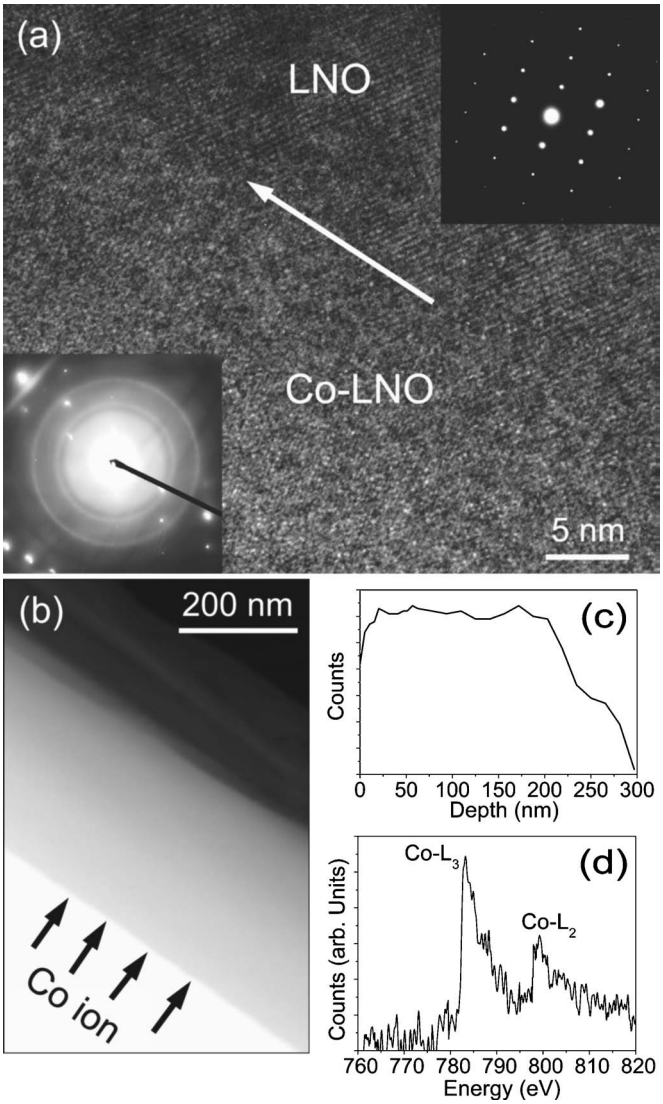

FIG. 1. (a) The HRTEM imaging of the $Co_{0.05}(LiNb)_{0.95}O_{3-\delta}$/LNO cross section shows the interface (white arrow) of the implanted layer and the wafer. Upper inset: The SAD pattern of the LNO wafer. Lower inset: The SAD pattern of a Co-implanted LNO layer. (b) The low magnification imaging of the cross-section specimens of the Co:LNO layer (gray) on the LNO wafer (dark gray). (c) The cross-sectional EDS. (d) The EELS show the Co $L_{2,3}$ of the Co-implanted LNO.

correlation part of the potential, we have used the energy- and position-dependent optical Hedin-Lundqvist potential with a muffin-tin radii overlap of 10% between contiguous spheres to simulate the atomic bond. These conditions have been found to produce good potentials for an accurate XANES calculation of complex transition metal oxides.[22–24]

The typical HRTEM imaging of the $Co_{0.05}(LiNb)_{0.95}O_{3-\delta}$/LNO cross-sectional specimen is shown in Fig. 1(a). There is no observation for the presence of Co metal (above 6 at. %) or Co-rich clusters in the overall of the implanted layer. From the upper inset of Fig. 1(a), one can see that the unimplanted LNO wafer is a single crystal. It is noted that ion implantation results in the structure transition of the implanted layer, i.e., polycrystalline structure, as shown in the lower inset of Fig. 1(a). This phenomenon indicates that the implantation process leads to the presence of structural defects. Figure 1(b) is the low magnification imaging of the cross-section implanted layer/wafer, revealing the uniform image of the implanted layer. EDS data taken at a number of locations throughout the specimens reveal a solid solution of Co dissolved in LNO with Co concentrations ranging from 4.4–5.3 at. %. As shown in Fig. 1(c), the cross-sectional EDS data shows that Co is uniformly distributed to a depth of ~220 nm with an average concentration of ~5 at. %. EELS were employed to probe the bonding characteristics. The EELS in Fig. 1(d) depicts the $L_{2,3}$ edge. Owing to the small concentration of the Co present in the film, the signal-to-noise ratio is small. Using Gauss peak fitting, a mixed valence state (2+ and 3+) of Co is found in the sample.[3] No significant variations are observed in EELS while performing line scans which indicate a homogeneous distribution of Co ions in the lattice.

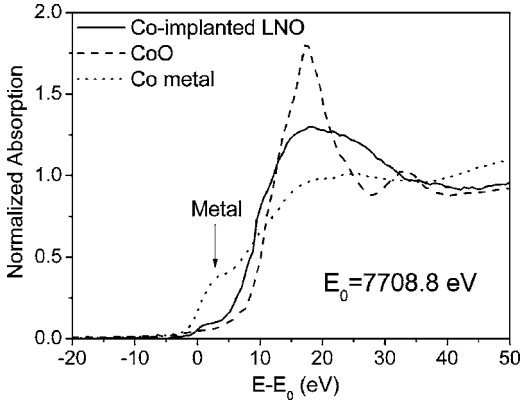

FIG. 2. Co K-edge XANES spectra for Co-implanted LNO with reference samples: Co metal and CoO.

Both Co^{2+} ions incorporating into the LNO lattice and CoO clusters may contribute to the Co^{2+} state in EELS results. In order to clarify the origin of the Co^{2+} state and infer something about the local structure, we have employed a Co K-edge XANES, which is much more sensitive to the local structure than a Co L-edge XANES.[5] Co K-edge XANES spectra from the Co:LNO and various reference materials (Co metal, CoO) are shown in Fig. 2. The plateau at $E-E_0=3$ eV ($E_0=7708.8$ eV) in the Co metal spectrum is unique to Co^0 and can be effectively used to determine the presence of Co metal, as marked in Fig. 2. This plateau is different from the weak pre-edge resonance observed at $E-E_0=0$ eV of the Co:LNO spectrum, which is not due to small quantities of Co^0, but rather to a $1s$ to $3d$ transition which is strictly dipole forbidden, but partially allowed when Co $3d$ and O $2p$ character in the first unoccupied state in the conduction band.[5,10] Besides, the absorption edge of the Co metal is a poor match to the Co:LNO due to the much lower threshold energy corresponding to the Co^0 state. Furthermore, an obvious difference of the XANES spectra between Co:LNO and CoO indicates that in a Co:LNO layer Co is not in the CoO form. From this comparison of a Co K-edge spectrum, we demonstrate that there is no evidence of Co metal and CoO throughout the implanted layer and Co^{2+} solutes into the LNO lattice.

The qualitative analysis of XANES spectra is sufficient to

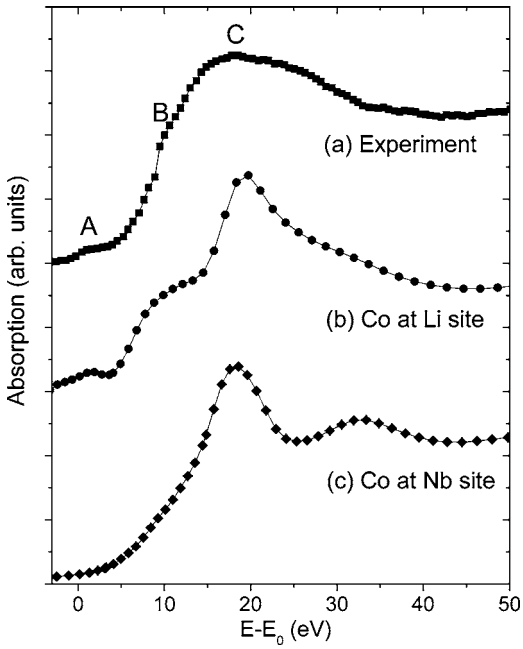

FIG. 3. (a) Co *K*-edge XANES spectrum for Co-implanted LNO. The MS calculations of the Co *K*-edge XANES spectra in (b) and (c) for center Co replacing Li and Nb sites, respectively.

explain the state of Co in LNO; it is, however, not sufficient to confirm the local geometry of Co^{2+}. Fortunately, the near-edge fine structures of the *K*-edge absorption spectra are the fingerprints of the local geometry around the absorbing atom, since it is driven by multiple correlation functions beyond the mere pair one.[22] The experimental Co *K*-edge XANES of Co-implanted LNO is compared in Fig. 3 with the *ab initio* calculated XANES using full MS theory. Figure 3(b) shows the calculated XANES spectrum of a Co atom replacing central Li. This is produced by a finite large cluster which contains 203 atoms within a radius of an 8 Å sphere from the central Co atom. The most interesting result here is the calculated spectrum displays three main features accurately replicating those of an experimental XANES spectrum, denoted by *A*, *B*, and *C* in order of increasing photon energy. In contrast to a Co atom substituting for central Li, we use a different atomic arrangement for the XANES spectrum in Fig. 3(c), i.e., Co substitution at central Nb. This spectrum corresponds to a cluster which contains 197 atoms within a radius of an 8 Å sphere from the central Co atom. One can see that the two main peaks at $E-E_0=18.4$ eV and $E-E_0=33.6$ eV are very clearly different from the three features in Figs. 3(a) and 3(b). Therefore, it is concluded that the Co^{2+} in LNO lies in a well-defined lattice position: the Li^+ lattice sites rather than Nb^{5+}. In addition, the XANES analysis confirms that the Co is surrounded by a distorted octahedral configuration, which is composed of two trigonal subshells.[17,18]

In general, the ferromagnet should have a high Curie temperature (T_C) above 500 K so that it can be used in a wide range of applications without temperature control.[6,25] Figure 4 presents the ferromagnetic behavior of Co:LNO recorded by a SQUID magnetometer for $5<T<350$ K and a VSM for $300<T<750$ K. As seen from this normalized ($M_T/M_{5\ K}$)

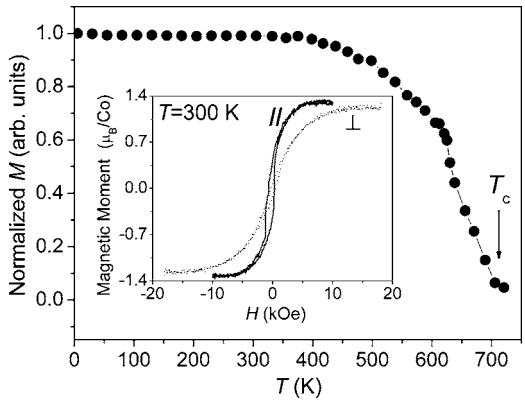

FIG. 4. The normalized ($M_T/M_{5\ K}$) *M-T* curve of $Co_{0.05}(LiNb)_{0.95}O_{3-\delta}$. The inset is the magnetic hysteresis loops at 300 K with the magnetizing field parallel (//) and perpendicular ($\perp$) to the implanted layer.

magnetization versus temperature (T) curve, the higher temperature (>300 K) magnetization shows a non-Brillouin-like behavior.[3,5] More interestingly, the Co:LNO system shows a high T_C of ~ 710 K. The inset of Fig. 4 shows magnetic hysteresis loops of Co:LNO measured at 300 K in a magnetic field (H) up to 10 kOe in a parallel direction and 18 kOe in a perpendicular direction to the implanted layer. It is useful to mention here that the magnetic properties of the unimplanted LNO and the sample holder are measured first with diamagnetlike magnetization, which are subtracted automatically by a computer during the measurement of Co:LNO. From the figure, one sees that the doping LNO show an in-plane easy axis of magnetization. Moreover, the magnetic moment is rather robust of 1.3 μ_B/Co-ion to the presence of structural defects, and parallel direction saturation magnetization is attained at 5 kOe with a coercive field at 660 Oe. Similarities to magnetic ordering were observed at temperature ≥ 250 K in three perovskites, $BaTiO_3$, $SrTiO_3$, and $KTaO_3$ when doped with Mn or Co by direct ion implantation.[8,26]

The magnetism can be explained by the interaction between bound magnetic polarons (BMP) in the case of either low carrier density or equivalently, strong carrier localization.[8,25] As indicated by the calculation of a XANES, the Co is mainly substitutional at Li sites, and HRTEM results show that the nonequilibrium process of ion implantation makes it possible that defects in the implanted layer are located throughout the lattice at arbitrary distances with respect to Co sites. According to Ref. 27, a donor spin of the defect strongly correlates with Co^{2+} within its orbit and can mediate effective interactions between them based on a Heisenberg exchange Hamiltonian. Consequently, the donors try to shape the BMP, coupling Co^{2+} within their orbits. Furthermore, the orbits tend to sufficiently spread out to overlap and interact with adjacent BMP to realize magnetic ordering.[25] In addition, in terms of the BMP mechanism, TC of dilute ferromagnetic oxides is described by[25]

$$T_C=[(S+1)s^2x\boldsymbol{\delta}/3]^{1/2}J_{ij}f_0(r_c^{eff}/r_0)^3/k_B, \qquad (1)$$

where S and s are the spin of the Co^{2+} and the donor, respectively, x is the doping concentration, $\boldsymbol{\delta}$ is the donor concen-

tration, J_{ij} is the *s-d* exchange parameter, f_0 is the oxygen packing fraction for the oxide ($LiNbO_3$), r_c^{eff} is the effective cation radius, and k_B is the Boltzmann's parameter. Using the parameters in the present case: $S=3/2$, $s=1/2$, $x=0.05$, $J_{ij}=3.8$ eV, $f_0=0.6$, $\delta=0.01$, $r_c^{eff}=0.20$ nm, $r_0=0.14$ nm;[25,27] the T_C given by Eq. (1) is then roughly estimated to be 786 K, which is close to the experimental results of 710 K.

It is well known that the LNO crystals show strong room temperature spontaneous polarization of 70 uC/cm^2, and ferroelectricity of LNO crystals can exist up to very high ferroelectric transition temperature T_E of 1483 K.[15] On the other hand, a high ferromagnetic Curie temperature T_c of 710 K are observed in Co:LNO. Accordingly, ferromagnetism and ferroelectricity may coexist in the present Co-implanted LNO system, similarly to the known multiferroic materials (e.g., $BiFeO_3$), possess promising ferromagnetic, ferroelectric properties, and a coupling between them.[20,28] More detailed work on the multiferroic properties of Co-implanted LNO with and without post-implant annealing is now in progress and will be reported separately.

In summary, employing the designed ion implantation, we have prepared a ferromagnetic oxide Co-doped LNO, where Co^{2+} is uniformly distributed to a depth of ~220 nm. Using complementary characterization and full multiple-scattering *ab initio* calculations of Co *K*-edge XANES spectra we unambiguously provide a structure fingerprint that Co^{2+} replaces Li^+ rather than Nb^{5+}. High temperature ferromagnetism ($T_C \sim 710$ K) and rather robust ferromagnetism of 1.3 μ_B/Co with an easy in-plane axis are observed in Co-implanted LNO. Ferromagnetism with a high T_C is realized in LNO which is already a material of great interest to application for ferroelectric devices, photorefractive devices, and surface acoustic wave filters. This may offer new approaches to the design of multifunctional ferromagnetic oxide that would facilitate the fabrication of new components in spintronic devices.

This work is supported in part by the National Natural Science Foundation of China (Grants No. 50325105 and No. 50371040). Assistance from the Institute of Semiconductors of Chinese Academy of Sciences and TEM Lab of Peking University is acknowledged.

*Author to whom correspondence should be addressed. Electronic address: panf@tsinghua.edu.cn

[1] I. Žutic, J. Fabian, and S. Das Sarma, Rev. Mod. Phys. **76**, 323 (2004).
[2] S. R. Shinde, S. B. Ogale, J. S. Higgins, H. Zheng, A. J. Millis, V. N. Kulkarni, R. Ramesh, R. L. Greene, and T. Venkatesan, Phys. Rev. Lett. **92**, 166601 (2004).
[3] S. B. Ogale, R. J. Choudhary, J. P. Buban, S. E. Lofland, S. R. Shinde, S. N. Kale, V. N. Kulkarni, J. Higgins, C. Lanci, J. R. Simpson, N. D. Browning, S. Das Sarma, H. D. Drew, R. L. Greene, and T. Venkatesan, Phys. Rev. Lett. **91**, 077205 (2003).
[4] B. Beschoten, P. A. Crowell, I. Malajovich, D. D. Awschalom, F. Matsukura, A. Shen, and H. Ohno, Phys. Rev. Lett. **83**, 3073 (1999).
[5] C. Song, K. W. Geng, F. Zeng, X. B. Wang, Y. X. Shen, F. Pan, Y. N. Xie, T. Liu, H. T. Zhou, and Z. Fan, Phys. Rev. B **73**, 024405 (2006).
[6] A. H. Macdonald, P. Schiffer, and N. Samarth, Nat. Mater. **4**, 195 (2005).
[7] W. Prellier, A. Fouchet, and B. Mercey, J. Phys.: Condens. Matter **15**, R1583 (2003).
[8] S. J. Pearton, W. H. Heo, M. Ivill, D. P. Norton, and T. Steiner, Semicond. Sci. Technol. **19**, R59 (2004).
[9] N. Theodoropoulou, A. F. Hebard, M. E. Overberg, C. R. Abernathy, S. J. Pearton, S. N. G. Chu, and R. G. Wilson, Phys. Rev. Lett. **89**, 107203 (2002).
[10] V. Shutthanandan, S. Thevuthasan, S. M. Heald, T. Droubay, M. H. Engelhard, T. C. Kaspar, D. E. McCready, L. Saraf, S. A. Chambers, B. S. Mun, N. Hamdan, P. Nachimuthu, B. Taylar, R. P. Sears, and B. Sinkovic, Appl. Phys. Lett. **84**, 4466 (2004).
[11] D. P. Norton, S. J. Pearton, A. F. Hebard, N. Theodoropoulou, L. A. Boatner, and R. G. Wilson, Appl. Phys. Lett. **82**, 239 (2003).
[12] J. S. Lee, J. D. Lim, Z. G. Khim, Y. D. Park, S. J. Pearton, and S. N. G. Chu, J. Appl. Phys. **93**, 4512 (2003).
[13] D. H. Kim, J. S. Yang, Y. S. Kim, D. -W. Kim, T. W. Noh, S. D. Bu, Y. -W. Kim, Y. D. Park, S. J. Peaton, Y. Jo, and J. -G. Park, Appl. Phys. Lett. **83**, 4574 (2003).
[14] M. A. Scarpulla, O. D. Dubon, K. M. Yu, O. Monteiro, M. R. Pillai, M. J. Aziz, and M. C. Ridgway, Appl. Phys. Lett. **82**, 1251 (2003).
[15] Y. Ohkubo, Y. Murakami, T. Saito, A. Yokoyama, S. Uehara, and Y. Kawase, Phys. Rev. B **65**, 052107 (2002).
[16] X. L. Hua, H. Ping, and H. Ping, J. Phys. Chem. Solids **66**, 918 (2005).
[17] M. G. Zhao and M. Chiu, Phys. Rev. B **49**, 12556 (1994).
[18] C. Prieto and C. Zaldo, Solid State Commun. **83**, 819 (1992).
[19] C. Prieto, C. Zaldo, P. Fessler, H. Dexpert, J. A. Sanz-García, and E. Diéguez, Phys. Rev. B **43**, 2594 (1991).
[20] J. Wang, J. B. Neaton, H. Zheng, V. Nagarajan, S. B. Ogale, B. Liu, D. Viehland, V. Vaithyanathan, D. G. Schlom, U. V. Waghmare, N. A. Spaldin, K. M. Rabe, M. Wuttig, and R. Ramesh, Science **299**, 1719 (2003).
[21] L. Rebouta, J. C. Soares, M. F. Da Silva, J. A. Sanz-García, E. Diéguez, and F. Agulló-López, Appl. Phys. Lett. **55**, 120 (1989).
[22] A. L. Ankudinov, B. Ravel, J. J. Rehr, and S. D. Conradson, Phys. Rev. B **58**, 7565 (1998).
[23] F. Farges, G. E. Brown, and J. J. Rehr, Phys. Rev. B **56**, 1809 (1997).
[24] Z. Y. Wu, S. Gota, F. Jollet, M. Pollak, M. Gautier-Soyer, and C. R. Natoli, Phys. Rev. B **55**, 2570 (1997).
[25] J. M. D. Coey, M. Venkatesan, and C. B. Fitzgerald, Nat. Mater. **4**, 173 (2005).
[26] J. S. Lee, Z. G. Khim, Y. D. Park, D. P. Norton, N. A. Theodoropoulou, A. F. Hebard, J. D. Budai, L. A. Boatner, S. J. Pearton, and R. G. Wilson, Solid-State Electron. **47**, 2225 (2003).
[27] P. A. Cox, *Transition Metal Oxides* (Clarendon Press, Oxford, 1992).
[28] W. Prellier, M. P. Singh, and P. Murugavel, J. Phys.: Condens. Matter **17**, R803 (2005).